The impact of iron sulfide on lead recovery at the giant Navan Zn-Pb orebody, Ireland

G.J Barker[a*1], A.R. Gerson[b], J.F. Menuge[a]

[a]UCD School of Geological Sciences, University College Dublin, Belfield, Dublin 4, Ireland, *Corresponding author. Tel: (+353) 1716 2141 E-mail address: Gareth.Barker1@gmail.com (G.J. Barker); J.F.Menuge@ucd.ie

[b]Minerals and Materials Science & Technology (MMaST), Mawson Institute, University of South Australia, Mawson Lakes, South Australia 5095, Australia Andrea.Gerson@unisa.edu.au

Abstract

It has been proposed that blending of Navan Conglomerate Group Ore (CGO) with Pale Beds Ore (PBO), the latter which floats well in isolation, results in sub-optimal Pb recovery with increased abundance of pyrite reporting to the concentrate and increased abundance of galena reporting to the tails.

QEMSCAN data indicate that poor liberation of galena particles is not the primary cause of sub-optimal recovery of galena. Rather, principal component analysis (PCA) of time of flight secondary ion mass spectrometry (ToF-SIMS) reveals that chemically altered surface species interfere with the selectivity and recovery of froth flotation indicating that there is some poisoning of galena mineral surfaces particularly with Fe-containing species possibly leading to loss of recovery. Analysis of the Pb-circuit cleaner tails indicates Pb-species association with sphalerite surfaces, as was observed for the flotation feed and rougher tails but with insufficient induced hydrophobicity by Pb-collector interaction for flotation. A small population of relatively clean galena surfaces is also observed which may result from low bubble-particle collision efficiency or insufficient liberation.

[1] Present address: Geological Survey of Northern Ireland, Colby House, Belfast, BT9 5BF, Northern Ireland

Fine-grained framboidal pyrite is the main diluting phase in the cleaner concentrate and is likely present due to entrainment. The presence of framboidal pyrite in CGO is of particular significance as its large surface area increases the rate of galvanic interaction with other metal sulfide minerals. We propose that increased abundance of refractory framboidal pyrite in CGO is the critical factor affecting the performance of the Navan Pb flotation circuit rather than purely high pyrite abundance.

1. Introduction

Base metal sulfides, such as galena and sphalerite, are one of the most important mineral groups and account for more than half of the world's metal production (Peng and Grano, 2010a). These valuable sulfides are often associated with gangue minerals including gangue sulfides (most commonly pyrite), oxides and silicates. The separation of value sulfide minerals from gangue minerals is most commonly achieved by froth flotation. Misplacement to value and waste streams is a common problem in flotation, which can be caused by inadequate liberation, mechanical entrainment or true flotation due to the properties inherent in the mineral or induced by contaminant species (Sui et al., 1997).

Minerals separation by flotation is a complex process and is dependent, along with other factors, on the relative distributions of hydrophobic (*e.g.* collector, polysulfide, elemental sulfide) and hydrophilic (*e.g.* metal hydroxide) species between different particles of the same mineral phase and between mineral phases (Piantadosi and Smart, 2002; Boulton et al., 2003). How a mineral surface changes during processing is critical to the outcome of flotation and many factors may influence the minerals' surface layers (Acres et al., 2010). During comminution a variety of surface reactions can take place such as oxidation, surface activation and galvanic interactions, which influence the mineral surface species. The resulting chemically altered surface layers are known to interfere with the selectivity and recovery of froth flotation designed for unreacted mineral surfaces (Smart et al., 2003).

Boliden Tara Mines Limited produce lead and zinc concentrates from the Navan Zn-Pb Irish-type deposit, County Meath, Ireland. The principal economic sulfides at Navan comprise sphalerite and galena averaging grades of 8 wt.% Zn and 2 wt.% Pb (Ashton et al., 1992). Base metal sulfides are accompanied by gangue minerals barite, calcite, dolomite and iron disulfide polymorphs pyrite and subordinate marcasite. The Navan deposit contains two ore types that are classified based on their hosting lithology. The majority (97 %) of ore is hosted by a series of Lower Carboniferous shallow-marine carbonates of Courceyan to Chadian age and is referred to as Pale Beds Ore (PBO) (Ashton et al., 1992). PBO has low iron disulfide (hereafter referred to as pyrite) content, typically 1-3 wt.% Fe but increasing in the upper lenses (Ashton et al., 1992). The remaining ore (3 wt.%), termed Conglomerate

Group Ore (CGO), is hosted by a sequence of debrite and fault talus referred to as Boulder Conglomerate. CGO differs from PBO in that it contains regions of abundant pyrite with variable morphological and chemical characteristics amounting to >20 wt.% of the total ore (Ashton et al., 1992). In a separate study Barker et al. (unpublished data) show that the CGO pyrite assumes various morphologies depending on its formational process and can contain differing amounts of minor element impurities, which may result in variable flotation response. A significant proportion of the pyrite is considered to be syngenetic framboidal pyrite containing small concentrations of minor element impurities. Other morphologies such as stalactitic and laminated are considered to be hydrothermal and contain greater concentrations of minor element impurities, such as arsenic up to 6 wt.%. Arsenic is shown to substitute for S in the CGO pyrite lattice, while Pb and Zn are interpreted to have been trapped as nanoparticles of co-precipitating galena and sphalerite, respectively (Barker et al., unpublished data).

Increased production from CGO lenses at Navan has resulted in an increased proportion of pyrite in the flotation feed. To minimize the impact of high Fe feed, CGO is always blended with PBO. Historically, in isolation PBO galena floats well with Pb recovery ≥70%. However, flotation of certain blended feeds can result in sub-optimal Pb recovery with increased abundance of pyrite reporting to the concentrate and increased abundance of galena reporting to the tails. It has been proposed that CGO with high pyrite content leads to increased contamination of mineral surfaces affecting galena flotation, with 10 to 15% lower Pb recovery (Barrie, pers. comm.).

The separation and flotation of galena from pyrite is known to be strongly dependent on the pyrite and galena surface metal oxidation species produced during comminution (Peng et al., 2003). Metal hydroxides present on mineral surfaces may render the minerals hydrophilic and decrease floatability or may induce interaction with collectors and enhance floatability (Sui et al., 1997). Iron oxidation species have been shown to depress both galena and pyrite flotation (Peng et al., 2003). Lead oxidation species can be responsible for the inadvertent activation of pyrite by Pb adsorbing to the pyrite surface and inadvertently forming a complex with the collector, inducing hydrophobicity (Smart, 1991; Finkelstein, 1997; Peng et al., 2003; Hart et al., 2006)

In this study we have investigated blended PBO and CGO flotation samples via a combined study of mineralogy, liberation, surface and microscopy analyses to determine whether hydrophilic poisoning occurs on the galena surfaces in the processing of blended feed.

2. Sample collection

Sampling was carried out during a period of blended ore flotation. Pulp samples were collected directly from the flotation feed, rougher tails, cleaner tails and cleaner concentrate of the Navan Pb flotation circuit (Figure 1). To inhibit continued oxidation and dissolution after removal from the circuit, samples were de-oxygenated by bubbling with oxygen-free nitrogen gas, sealed, quickly frozen and thereafter stored in a freezer prior to ToF-SIMS surface analysis. This collection procedure reduces uncertainty in the relationship between measured surface speciation and those prevailing in the original pulp of the flotation circuit (Smart, 1991).

3. Analytical methods

For QEMSCAN analyses solid samples from the flotation feed, cleaner tails and cleaner concentrate were cyclosized into seven sub-samples which were combined into three discrete size fractions using cones 1, 3 and 5. The resulting size fractions are mineral specific gravity (SG) sensitive. Assuming an SG of quartz (2.7) the resulting size fraction would be +42 μm, -42 to +23 μm and -23 to +12 μm, whilst for galena (SG 7.5) the respective resulting size fractions would be +22 μm, -22 to +12 μm and -12 to +6 μm. We use hereafter the size fractions assuming a SG of quartz. However, for samples with high galena content, *e.g.* cleaner concentrate (79 wt.% galena), the actual fraction sizes will be smaller than indicated. Each sample size fraction was split using a rotary micro-riffler to produce a representative sub-sample that was mounted in epoxy resin, ground, polished and carbon coated prior to QEMSCAN examination.

ToF-SIMS analyses were undertaken in order to examine the surface species on the solids retrieved from Pb-circuit flotation feed, rougher tails, cleaner tails and cleaner concentrate. ToF-SIMS spectra were acquired from the same five areas per sample, from 0 to 500 m/z using a PHI TRIFT V nanoTOF spectrometer at University of South Australia. Multiple areas were chosen to ensure the analyses covered

enough particles, both large and small, for reliable principal component analysis (PCA). The size of the analyses areas were varied as follows: flotation feed 450 × 450 μm, rougher tails 500 × 500 μm, cleaner tails 250 × 250 μm and cleaner concentrate 250 × 250 μm, in order to keep the numbers of particles sampled roughly equivalent.

The software package PLS Toolbox 6.7.1 from Eigenvector Research Ltd. (Manson, Washington State, U.S.A.) running on Matlab 7.13 was used for the PCA analysis. The resulting factor loadings (correlation factors) represent the statistical correlation for each mass for that specific principal component (PC). This analysis therefore enables the identification of all the species correlated to a particular mineral phase as recognized by its elemental signature, *e.g*. Pb for galena. At each pixel at each region a positive mass fragment data set is collected in a map across the region, followed by collection across the same region of a negative ion dataset. The positive or negative ion data across the five regions of analyses were first concatenated, in the same order, to form a strip, *i.e*. attached along the *x*-dimension. The two strips representing the positive ion and negative ion data were then concatenated in the *z*-dimension. Thus, each region of positive ion data was associated with the representative negative ion data from the same region and PCA analysis of all data, positive and negative, from any one sample was undertaken simultaneously. This represents an improved methodology over that used previously (*e.g*. Gerson et al., 2012) where the emphasis has been on analysis of positive ion species only and no statistical correlation of positive and negative species has been attempted.

PCA analysis for each fully concatenated data set was carried out using data that had previously been normalized and scaled. Auto scaling, in which the mean centred variable is divided by the standard deviation of the intensity for that specific mass peak, puts all variables on an equal basis in the analysis. Thus, the less intense but potentially more chemically significant higher mass peaks receive the same level of consideration on mean centred analysis as the intense, low mass peaks.

The first principal component (PC 1) is associated with large topographic and matrix variations (ion yield variations across the sample) in the data and accounts for as much of the variability in the data as possible. After this data is removed, each subsequent PC analyses the remaining data for correlations, which may be either correlated or anti-correlated. Successive PCs describe the correlations of the various

constituents (valuable mineral phases and other materials, *e.g*. gangue) within the imaged data in order of importance. These PCs are then relatively free of topographic and matrix effects. Factor loadings for each PC were ordered from smallest (*i.e*. most negative) to largest and those species with absolute factor loading value less than 0.1 were discarded as having little significant correlation within that specific PC.

4. Flotation results

On the day of sampling the Pb flotation circuit received 7,500 tons of blended ore containing 5 wt.% Zn, 1.3 wt.% Pb and 4.6 wt.% Fe. The daily Pb recovery was calculated at 62.4%, whereas the monthly averaged data showed lower Pb recovery of 59.5%. The monthly averaged Pb recovery is 10.5% below the average Pb recovery achieved when PBO is floated in isolation. Figure 2, which shows the Pb recovery by size for all size fractions measured at Navan for the month that sampling took place, also shows that there is no Pb recovery at sizes greater than 75 μm size fraction.

5. QEMSCAN results

5.1 Modal mineralogy

Sulfide minerals account for 32 wt.% of the flotation feed (Table 1) with pyrite present at 16.1 wt.%, followed by sphalerite with 12.6 wt.% and galena 3.5 wt.% (Table 1). The main sulfide minerals are found in greatest abundance in the coarsest +42 μm size fraction (Table 2). The principal non-sulfide gangue minerals in the flotation feed are calcite (26.3 wt.%) and dolomite (13.8 wt.%), while quartz, feldspars and barite also contribute > 5 wt.% each to the feed (Table 1). This blended ore, non-sulfide gangue mineralogy is comparable with the mineralogy determined previously for PBO flotation feed samples (Boliden Tara Mines Limited internal reports).

The Pb-circuit cleaner tail sample is dominated by sulfides, which account for in excess of 80 wt.% (Table 1). Calcite is the predominant non-sulfide gangue mineral and accounts for 5.3 wt.% of the tails sample. The overwhelming majority of the sample is represented by pyrite (68.3 wt.%), which was mostly found in the two finest sample fractions, -42 to +23 μm an -23 to +12 μm (Table 2). A total of 7.0 wt.% galena (Table 1) was lost to the cleaner tails with approximately equal distribution between size fractions (Table 2).

The Pb-circuit cleaner concentrate sample is dominated by galena accounting for 79.4 wt.% (Table 1). The greatest content was observed in the -42 to +23 μm size fraction with 42.4 wt.% (Table 2) with pyrite at 16.0 wt.% (Table 1) being mostly found in the -23 to +12 μm size fraction (Table 2).

5.2. Liberation and mineral associations

Liberation data of pyrite and galena measured from all size fractions for the cleaner concentrate and tails are presented in Table 2 and Figure 3. Liberated grains are defined as any particle containing between 90 % and 100 % by area of the mineral of interest. Particles that contain between 30 % and 90 % by area are referred to as middling particles, whilst those containing less than 30 % by area are referred to as locked particles.

The majority of the pyrite across all three size fractions for the three samples, feed, cleaner tails and cleaner concentrate is liberated with the exception of the +42 μm cleaner concentrate (Table 2, Figure. 3A). In the flotation feed sample the majority of the pyrite (62.0 %) is found in the +42 μm size fraction (Table 2). In the cleaner tails pyrite is found predominantly in the -42 to +23 μm and -23 to +12 μm size fractions whereas in the cleaner concentrate pyrite is found predominantly (70.4 %) in the fine -23 to +12 μm fraction (Table 2). QEMSCAN images of liberated pyrite particles in the cleaner concentrate -23 to +12 μm size fraction are predominantly spherical in appearance. SEM analysis of this size fraction revealed that the overwhelming majority of pyrite reporting to the concentrate stream had spheroidal or framboidal morphology (Figure 4). Pyrite in the flotation feed and cleaner tails samples shows similar mineral association characteristics with the majority of non-liberated particles associated with carbonates (Table 2).

In the flotation feed the majority of the galena occurs in the +42 μm size fraction contributing, in a liberated form, 31.4 % of the total galena (Table 2). A large number of galena particles host boulangerite, which accounts for 45.0 % of the total galena across all size fractions giving a combined liberated galena plus galena-boulangerite value of 87.5 % of the galena in the flotation feed. Locked galena particles are preferentially associated with sulfide minerals rather than non-sulfide gangue. Liberation is poorer in the cleaner tails than the feed with more of the liberated galena occurring in the finest -23 to +12 μm size fraction as compared to the

other two size fractions (Fig. 3B). Boulangerite-bearing galena also accounts for a significant amount (22.4 %) of galena in the cleaner tails. The majority of locked galena particles in the cleaner tails occur with sphalerite (19.2 %), followed by pyrite (8.1 %). The greatest liberation of galena in the cleaner concentrate sample occurs in the -42 to +23 μm size fraction accounting for 19.3 % of all galena (Table 2). Boulangerite–bearing galena particles are the most abundant phase in the cleaner concentrate. Galena particles that are locked are primarily associated with sulfides rather than non-sulfide gangue.

6. ToF-SIMS results

ToF-SIMS was used to identify trends in surface chemical speciation affecting the selectivity and separation of galena from pyrite (and other gangue minerals) during flotation. Principal components subsequent to PC 1 that provide the most explicit recognition of galena surfaces (Pb signals) were compared between Pb-circuit flotation feed, rougher tails, cleaner tails and cleaner concentrate samples. For each PC, surface species that are spatially correlated are grouped as having either positive or negative factor loadings. The factor loadings for particular species in each set are not intensity comparisons but factors giving the strength of the statistical correlation of the masses (species) in that set of data.

Figure 5A shows PCs 3, 4 and 5 for the flotation feed in which factor loadings (multiplied by the % of each data accounted for by each PC to enable better comparison) for Pb were significant. These three PCs were also the only PCs to register the presence of Zn. The greatest degree of correlation, for both PCs 3 and 4, is between the Pb isotopes and the Zn isotopes. For PC 3 there is also correlation with S, SO, Ba, BaOH and Cu. For PC 4 there is additional correlation between the Pb and Fe isotopes as well as Ca, CaOH and Cu. Images illustrating the correlation between Cu, Zn and Pb are provided in Figure 6. On examination of the PC images for PC 3 and PC 4 it is apparent that the particles with positive factor loading in PC 3 are also represented by the combination of positive and negative factor loadings in PC 4. It is suggested on the basis of the significant distributions of these factor loadings in the PC images, in relation to the relative occurrences of sphalerite (12.6 wt.%) and galena (3.5 wt.%), that PC3 and PC 4 may predominantly be due to surface adsorbed species on sphalerite. The scaled factor loading for the Pb isotopes for PC 5 are much

smaller than for either PC 3 or 4 and are highly correlated to Fe isotopes, FeS and FeOH as well as Ca, CaOH and to a lesser extent Ba and BaOH. Figure 6 provides an example of where Pb is not correlated to either Zn or Cu as is the case for PC 5. We suggest that the positive factor loadings for PC 5 are due to Fe adsorption onto galena rather than Pb adsorption onto pyrite due to the widespread occurrence of Fe-species across the images but the much more limited occurrence of Pb-containing areas correlating to the regions of positive factor loading of PC 5.

The results of the PCA ToF-SIMS analysis for the rougher tails are shown in Figure 5B for the significant principal components with Pb. PC 3 shows significant correlation between Pb isotopes, Zn isotopes and Cu. The widespread distribution of areas with positive factor loading on examination of PC 3 images suggests adsorbed Pb species on sphalerite, as for PC3 and PC4 from the feed analysis. Strong anti-correlation is observed with Ba and oxidised S species which are suggestive of barite. The only other principal component to show significant Pb was PC 5. In this instance the Pb isotopes are correlated with Fe species, including FeS, and various gangue mineral cations. There is also minor anti-correlation to the Zn isotopes (Zn -0.051; ^{66}Zn -0.045; ^{68}Zn -0.035); however these factor loadings are smaller than the cut-off for values displayed in Figure 5. On examination of the individual species maps it is clear that Fe (and Fe species) are also widely distributed in regions not corresponding to a positive factor loading for PC 5 and that, in addition, the signal from +FeS is extremely weak. We therefore propose that this PC arises from surface contamination, mainly by Fe species and gangue cations, of galena surfaces causing misreporting to the rougher tails.

PCs 3, 4 and 5 for the ToF-SIMS data from the Pb-circuit cleaner tails (Figure 5C) also show significant Pb correlation. PC 3 shows strong correlation between the Pb isotopes and Zn isotopes with more minor correlation to S, Fe and CaOH. This set of correlations bear greatest resemblance to PC 4 from the flotation feed and PC 3 from the rougher tails, which were suggested to represent adsorption of Pb species adsorbed onto sphalerite. PC 4 for the cleaner tails shows anti-correlation between the Pb and Zn isotopes with correlation of the Pb isotopes to CaOH, various Fe isotopes and CN. This PC is similar in nature to PC 5 from the flotation feed and from the rougher tails which was suggested to represent Fe species adsorbed onto galena. PC 5 for the cleaner tails seems to indicate a relatively clean galena surface (minor correlation to Fe) with significant anti-correlation to FeS and FeO_2 species.

PCA analysis of the ToF-SIMS data from the cleaner concentrate shows Pb in PCs 2, 3 and 4, with Zn only being significant in PC 4 (Figure 5D). In PC 2 the Pb isotopes are correlated to various positive species including the Fe isotopes but notably not FeS or FeO_2 suggesting the presence of adsorbed dissolved species rather than pyrite surfaces. This would seem to be due to partial dissolution of gangue minerals but with insufficient adsorption of hydrophilic species to inhibit flotation. In PC 3, the most significant PC for Pb, the Pb isotopes show correlation to S and oxidised S species indicating relatively clean galena surfaces. In PC 4 there is correlation between the Pb isotopes with very significant correlation to FeO and FeS. However, the signals for these species are extremely weak and widely dispersed across the analysis area. These observations are similar to PC 5 for the feed and rougher tails and PC 4 for the cleaner tails and suggest Fe species adsorbed onto galena. There is anti-correlation of the Pb isotopes to the Zn isotopes which most likely represent sphalerite surfaces, which show significant correlation to Cu. Notably for the Pb-circuit cleaner concentrate Zn does not show significant correlation in either PC 2 or PC 3 and is anti-correlated to the Pb isotopes in PC 4.

7. Discussion

As the rest potential of galena (0.40 V SHE) is less than that of either pyrite (0.66 V SHE) or sphalerite (0.46 V SHE) (Majima, 1969), galena when in galvanic contact with these minerals will tend to oxidise preferentially (Peng et al., 2003; Chandra and Gerson, 2009; Payant et al., 2012; Rao and Finch, 1988; Kwong et al., 2003). Oxidation of the anodic mineral is frequently accompanied by the dissolution and re-adsorption of its metal ion(s) onto the original mineral and the surface of other minerals (Cullinan et al., 1999). Previous studies have shown that the larger the ratio of cathodic mineral to anodic mineral surface area, the greater the galvanic interaction (Kwong et al., 2003; Yelloji Rao and Natarajan, 1989). The large surface area CGO framboidal pyrite morphology may result in increased galvanic interactions with galena resulting in greater release of Pb-containing species (Figure 7) and increased likelihood of re-adsorption of these species onto other sulfide minerals. This process could result in inadvertent Pb activation of both pyrite and sphalerite resulting in misreporting to the Pb concentrate (Basilio et al., 1996; Peng et al., 2012).

Despite pyrite being nobler than galena and sphalerite its oxidation is unavoidable during blasting and grinding. Framboidal pyrite and associated loose < 2

μm euhedral microcrystalline grains, which occur in abundance in CGO, have large surface area and will oxidise at a much greater apparent rate (up to 10× faster) than more blocky textures producing a variety of Fe oxidation products (Smart pers. comm.). Certain CGO pyrite may also contain significant minor element impurities and deviations in stoichiometry resulting in variations in semiconducting properties and increased oxidation (Barker et al., unpublished data). Fe species in the process water may also come from recycled process water, which can contain significant mineral dissolution and oxidation products.

Iron contamination of galena surfaces is known to play a dominant role in depressing galena flotation while Pb oxidation species have little effect on galena flotation (Peng et al., 2003; Peng and Grano, 2010a). Recent studies show that the interaction of Fe hydroxide colloids with galena particles depends on the degree of galena surface dissolution (Peng and Grano, 2010c). Unoxidised galena may be electrostatically repulsed from Fe oxidation species, while oxidized galena is attracted to Fe oxidation species (Peng and Grano, 2010b). Electrostatic interaction of Fe oxidation species with Pb oxidation species could be a contributing factor to the adsorption of Fe oxidation species on galena and subsequent depression during flotation. Consequently, oxidation and dissolution of galena, resulting from galvanic interactions, enhances adsorption of Fe oxidation species on the surface, acting to depress the galena.

Table 2 shows that more than 75% of galena entering the circuit is in the +45 μm size fraction, compared with only 34.1% in the cleaner concentrate. This indicates that there has been significant depression of galena in the coarsest size fraction in agreement with Senior and Trahar (1991). Peng and Grano (2010c) suggest that with an increase in the amount of Fe hydroxide colloids the flotation of fine galena particles is depressed significantly as Fe hydroxide colloids are more adsorbed on finer particles than intermediate sized particles. It is possible that surfaces of fine galena particles are more easily oxidised than surfaces of larger particles (Peng and Grano, 2010b). Thus, Fe oxidation species are preferentially adsorbed on the finer galena particles accounting for the depression in flotation of finer liberated particles. Johnson (2006) also suggests that the flotation recovery of liberated valuable minerals in the fine size fraction would be affected detrimentally to a greater extent than the intermediate fraction by the presence of the Fe hydroxides.

These effects have been attributed to increased surface area but may also be the result of finer particles having a higher surface energy per unit area (Sivamohan, 1990). However, the depression of fine galena particles may not be related to hydrophilic contamination but could be ascribed to the lowered momentum of small particles, which affect their behaviour in particle–bubble collisions (Johnson, 2006) or lower probability of fine particles combining with gas particles (Boulton et al., 2003). CGO framboidal pyrite occurs interbedded with argillaceous calcsiltite and is interpreted to be similar to the naturally floating, carbonaceous pyrite described for Mount Isa (Young et al., 1997). Carbonaceous pyrite at Mount Isa is hydrophobic under almost any flotation conditions and consumes large quantities of reagent, making flotation difficult to control (Young et al., 1997). If CGO framboids share the same flotation behaviour then the natural hydrophobicity of carbonaceous framboidal pyrite may also account for it misreporting to the Pb cleaner concentrate.

The flotation data for the month of sampling reveals that the Pb recovery for blended ore was 10.5 % below that of PBO floated in isolation, indicating that a particular characteristic of CGO is detrimental to Pb recovery. QEMSCAN revealed that in excess of 87 % of galena entering the flotation circuit is liberated or is associated with boulangerite-bearing particles suggesting that galena liberation is not a significant factor in sub-optimal recovery.

PCA ToF-SIMS analysis of the flotation feed shows strong correlation of Pb and Zn (PC 3 and 4, Figure 5A) suggesting, due to the significant distribution of positive regions of these PCs, adsorption of dissolved Pb species onto sphalerite. These PCs also show a correlation with Cu, which has been shown to be enriched in certain sphalerites at Navan, which were precipitated from deep, hydrothermal fluids (Gagnevin et al., 2014). We propose, due to the similarity of distribution of positive factor loadings in the resulting PC images for PC 3 and PC 4 that the positive correlation of Fe, Pb and Zn isotopes in PC 4 is due to adsorption of both dissolved Fe and Pb species onto sphalerite surfaces, whereas the correlation of Pb and Zn isotopes in PC 3 is due only to the adsorption of Pb-isotopes onto sphalerite. The high degree of correlation of Fe in PC 5 to Pb species appears to indicate Fe adsorption onto galena surfaces rather than Pb adsorption onto pyrite as there exists a wide distribution of Fe, likely arising from pyrite, not associated with Pb. At this time there is no apparent reason why Pb should adsorb onto specific grains of pyrite rather than across the whole pyrite population.

For the rougher tails two Pb isotope containing PCs are observed, PC 3 and 5 (Figure 5B). These are similar in nature, respectively, to PC 4 and PC 5 from the feed analysis suggesting particle populations of sphalerite with surface adsorbed Pb and galena with surface adsorbed Fe-species and gangue cations. These conclusions suggest some degree of Pb activation/adsorption of sphalerite surfaces but insufficient to result in flotation, possibly due to co-adsorption of hydrophilic species. In addition hydrophilic species adsorption onto galena may result in surface 'poisoning' resulting in loss of recovery.

Galena is lost to the cleaner tails with relatively even distribution across all size fractions as liberated > middling > locked particles (Figure 3B). Liberated galena is predominantly found in the finest -23 to +12 μm size fraction. These results indicate that poor liberation is not a primary control on misplacement of galena to the cleaner tails stream. For galena in the Pb-circuit cleaner tails there is again significant correlation between the Pb and Zn isotopes (PC 3, Figure 5C) possibly, as proposed for the flotation feed and rougher tails, resulting from Pb-containing species transfer from galena to sphalerite particles. There is also, as for PC 5 for the flotation feed, considerable correlation between Pb and Fe-containing species (PC 4, anti-correlated to Zn, Figure 5C) and examination of the mass fragment images confirms that PC 3 and PC 4 for the cleaner tails represent two distinct particle populations. Even though pyrite is the dominant mineral within the cleaner tail (67.8 wt.%) it appears from the PCA analysis in comparison with the PCA image and individual species images that, as for the flotation feed and rougher tail (PC 5 in both instances), this principal component arises from Fe-species adsorption onto galena.

QEMSCAN results show that over half of all liberated galena in the cleaner tails stream is in the -23 to +12 μm size fraction (Table 2). The misreporting of finer liberated galena particles to the tails stream may be due to the ratio of hydrophobic and hydrophilic species on the galena surface resulting from a greater propensity for surface oxidation and adsorption of Fe hydroxide colloidal particles as discussed above. The Pb population shown by PC 5 shows poor correlations suggesting relatively clean galena surfaces reporting to the tails stream. This suggests that some fine, clean galena particles may fail to float due to low bubble-particle collision efficiency. It is also possible that this PC corresponds to insufficiently liberated galena particles.

In the Pb-circuit cleaner concentrate pyrite is the main diluting mineral accounting for 16.0 wt.% of the total sample. The majority of pyrite in the +42 μm size fraction of the cleaner concentrate occurred as middling and locked particles (Figure 3A). Over 60 % of the locked pyrite particles (9 % of all pyrite) in the cleaner concentrate are in association with galena, which may account for pyrite's flotation behaviour. However, mineral liberation data indicates that 85 % of the pyrite in the Pb-circuit flotation concentrate is liberated, indicating that poor liberation of pyrite is not the primary cause of its flotation. Size distribution data reveals that pyrite is particularly abundant in the finest -23 to +12 μm size fraction with 70 % of all pyrite reporting to this size fraction. The enrichment of pyrite in the fines results in a drop in galena abundance from 95 % to 59 % in the +42 μm to the -23 to +12 μm size fraction, respectively. SEM analyses reveal that framboidal pyrite is preferentially floated into the concentrate (Figure 4). Framboidal pyrite makes up a large proportion of the CGO pyrite and is rarely found in PBO. Framboids have a size range of 3 – 25 μm and are composed of discrete microcrystals that vary in size between 0.1 and 1.8 μm. Grinding is likely to result in disseminated framboids and possibly the disaggregation of their constituent microcrystals. Hence, the predominance of fine-grained framboidal pyrite in the Pb cleaner concentrate is likely in large part due to entrainment.

There are numerous associations of Pb with various cations (Na, Mg, Al, Si, K, Ca, Ba, Fe) indicated by PC 2 for the Pb-circuit cleaner concentrate (Figure 5D) although the factor loadings for the Pb isotopes are not large. Examination of the species maps suggests that positive correlations for this PC are widespread. This would seem to be due to partial dissolution and re-adsorption of gangue minerals but with insufficient adsorption of hydrophilic species to inhibit flotation. Anti-correlation to S species is evident in this PC. However, it is likely that these S-species are associated with relatively clean galena surfaces. PC 3 shows relatively clean Pb-containing surfaces with correlation only to some S-containing species.

Pb species as indicated by PC 4 are highly correlated to FeS and FeO_2 and are anti-correlated to Zn isotopes which are correlated to Cu, possibly indicating Cu inclusion in sphalerite (Gagnevin et al., 2014). We propose this observation is due to Fe-species adsorption onto galena surfaces due to the reasons given previously, as

was also observed for the feed (PC 3 and 4), rougher tails (PC 3) and cleaner tails (PC 3).

8. Conclusion

QEMSCAN data indicate that poor liberation of galena particles is not the primary cause of sub-optimal recovery of galena. Rather, ToF-SIMS reveals that chemically altered surface species interfere with the selectivity and recovery of froth flotation indicating that there is some poisoning of mineral surfaces. Hydrophilic oxidation products could originate from a number of sources including rapidly oxidising CGO framboidal pyrite, galvanic interactions or contaminants present in process water. Galvanic interaction and oxidation of metal sulfides apparently occurs prior to entering the Pb flotation circuit with feed samples showing both sphalerite surfaces with a high degree of surface contamination, principally from dissolved Pb-containing species and galena surfaces contaminated by surface adsorbed Fe-species. Preferential oxidation of galena, prior to either sphalerite or pyrite, is predicted on the basis of examination of galvanic interactions.

Analysis of the Pb-circuit tails indicates Pb-species association with sphalerite as was observed for the flotation feed and rougher tails. However, insufficient hydrophobicity is induced by Pb-collector interaction for flotation. A small population of relatively clean galena surfaces is also observed which may result from low bubble-particle collision efficiency or insufficient liberation.

The galena in the Pb-circuit cleaner concentrate sample shows no association with dissolved Zn species. Fine-grained framboidal pyrite is the main diluting phase in the concentrate and is likely to be present due to entrainment.

We propose that blending of high Fe CGO with PBO affects the performance of the Pb flotation circuit in a number of ways. Under mixed mineral conditions galvanic interactions between metal sulfides will increase and selectivity and flotation of galena will decrease. The presence of framboidal pyrite in CGO is of particular significance as its large surface area is likely to result in increased rate of galvanic interaction with other metal sulfide minerals. CGO pyrite may also misreport to the Pb cleaner concentrate due its fine grain size and refractory nature. We propose that increased abundance of refractory framboidal pyrite in CGO is the critical factor affecting the performance of the Navan Pb flotation circuit rather than purely high pyrite abundance.

Acknowledgements

We thank Boliden Tara Mines Limited for permission to collect samples and publish these results. We gratefully acknowledge the funding from Boliden Tara Mines Limited and the Irish Research Council for GJB's PhD project. Thanks to Colm Rice from Tara Mines for assistance with sample collection. We would also like to thank Dr. John Denman and Ms. Zofia Swierczek (both of IWRI, University of South Australia) for the ToF-SIMS and QEMSCAN measurements, respectively.

References

Acres, R.G., Harmer, S.L., Beattie, D.A., 2010. Synchrotron XPS, NEXAFS, and ToF-SIMS studies of solution exposed chalcopyrite and heterogeneous chalcopyrite with pyrite. Miner. Eng. 23, 928–936.

Ashton, J.H., Black, A., Geraghty, J., Holdstock, M., Hyland, E., 1992. The geological setting and metal distribution patterns of Zn-Pb-Fe mineralization in the Navan Boulder Conglomerate. In: The Irish Minerals Industry 1980-1990. Irish Association for Economic Geology, Dublin, pp. 171–210.

Barker, G.J., Menuge, J.F., Blakeman, R.J., Unpublished results. Significance of textural and chemical variation of FeS_2 from the Boulder Conglomerate of the Navan Zn-Pb deposit, Ireland.

Basilio, C., Kartio, I., Yoon, R.-H., 1996. Lead activation of sphalerite during galena flotation. Miner. Eng. 9, 869–879.

Boulton, A., Fornasiero, D., Ralston, J., 2003. Characterisation of sphalerite and pyrite flotation samples by XPS and ToF-SIMS. Int. J. Miner. Process. 70, 205–219.

Chandra, A.P., Gerson, A.R., 2009. A review of the fundamental studies of the copper activation mechanisms for selective flotation of the sulfide minerals, sphalerite and pyrite. Adv. Colloid. Interfac. Science 145, 97–110.

Cullinan, V.J., Grano, S.R., Greet, C.J., Johnson, N.W., Ralston, J., 1999. Investigating fine galena recovery problems in the lead circuit of Mount Isa Mines Lead/Zinc Concentrator part 1: Grinding media effects. Miner. Eng. 12, 147–163.

Finkelstein, N.P., 1997. The activation of sulphide minerals for flotation: a review. Int. J. Miner. Process. 52, 81–120.

Gagnevin, D., Menuge, J.F., Kronz, A., Barrie, C.D., Boyce, A.J., 2014. Minor Elements in Layered Sphalerite Record Fluid Origin in the Giant Navan Zn-Pb Orebody, Ireland. Economic Geology, in press.

Gerson, A.R., Smart, R.S.C., Li, J., Kawashima, N., Weedon, D., Triffett, B., Bradshaw, D., 2012. Diagnosis of the surface chemical influences on flotation performance: Copper sulfides and molybdenite. Int. J. Miner. Process. 106–109, 16–30.

Hart, B., Biesinger, M., Smart, R.S.C., 2006. Improved statistical methods applied to surface chemistry in minerals flotation. Miner. Eng. 19, 790–798.

Johnson, N.W., 2006. Liberated 0–10 μm particles from sulphide ores, their production and separation—Recent developments and future needs. Miner. Eng. 19, 666–674.

Kwong, Y.T.J., Swerhone, G.W., Lawrence, J.R., 2003. Galvanic sulphide oxidation as a metal-leaching mechanism and its environmental implications. Geochem.: Explor. Environ., Anal. 3, 337–343.

Majima, H., 1969. How oxidation affects selective flotation of complex sulphide ores. Can. Metall. Q. 8, 269–273.

Payant, R., Rosenblum, F., Nesset, J.E., Finch, J.A., 2012. The self-heating of sulfides: Galvanic effects. Miner. Eng. 26, 57–63.

Peng, Y., Grano, S., Fornasiero, D., Ralston, J., 2003. Control of grinding conditions in the flotation of galena and its separation from pyrite. Int. J. Miner. Process. 70, 67–82.

Peng, Y., Grano, S., 2010a. Inferring the distribution of iron oxidation species on mineral surfaces during grinding of base metal sulphides. Electrochim. Acta 55, 5470–5477.

Peng, Y., Grano, S., 2010b. Effect of iron contamination from grinding media on the flotation of sulphide minerals of different particle size. Int. J. Miner. Process. 97, 1–6.

Peng, Y., Grano, S., 2010c. Dissolution of fine and intermediate sized galena particles and their interactions with iron hydroxide colloids. J. Colloid Interface Sci. 347, 127–131.

Peng, Y., Wang, B., Gerson, A., 2012. The effect of electrochemical potential on the activation of pyrite by copper and lead ions during grinding. Int. J. Miner. Process. 102–103, 141–149.

Piantadosi, C., Smart, R.S., 2002. Statistical comparison of hydrophobic and hydrophilic species on galena and pyrite particles in flotation concentrates and tails from TOF-SIMS evidence. Int. J. Miner. Process. 64, 43–54.

Rao, S.R., Finch, J.A., 1988. Galvanic Interaction Studies on Sulphide Minerals. Can. Metall. Q. 27, 253–259.

Senior, G.D., Trahar, W.J., 1991. The influence of metal hydroxides and collector on the flotation of chalcopyrite. Int. J. Miner. Process. 33, 321–341.

Sivamohan, R., 1990. The problem of recovering very fine particles in mineral processing — A review. Int. J. Miner. Process. 28, 247–288.

Smart, R.S.C., 1991. Surface-layers in base-metal sulfide flotation. Miner. Eng. 4, 891–909.

Smart, R.S.C., Amarantidis, J., Skinner, W.M., Prestidge, C.A., Vanier, L., Grano, S.R., 2003. Surface analytical studies of oxidation and collector adsorption in sulfide mineral flotation. In: Wandelt, K., Thurgate, S. (Eds.), Solid—Liquid Interfaces. Springer Berlin Heidelberg, Berlin, Heidelberg, pp. 3–62.

Sui, C.C., Brienne, S.H.R., Xu, Z., Finch, J.A., 1997. Xanthate adsorption on Pb contaminated pyrite. Int. J. Miner. Process. 49, 207–221.

Yelloji Rao, M.K., Natarajan, K.A., 1989. Electrochemical effects of mineral-mineral interactions on the flotation of chalcopyrite and sphalerite. Int. J. Miner. Process. 27, 279–293.

Young, M.F., Pease, J.D., Johnson, N.W., Munro, P., 1997. Developments in Milling Practice at the Lead/Zinc Concentrator of Mount Isa Mines Limited from 1990. AusIMM Sixth Mill Operators Conference, 6-8 October 1997 Madang, Papua New Guinea, pp. 133-139.

Figure captions

Figure 1. Schematic diagram showing Navan lead flotation circuit and sampling points: (A) flotation feed; (B) rougher tails; (C) cleaner tails and; (D) cleaner concentrate.

Figure 2. Recovery by size fraction, for the month of sampling, for the Navan lead flotation circuit.

Figure 3. Comparison of particle liberation determined by QEMSCAN for (A) pyrite in the cleaner concentrate and (B) galena in the cleaner tails.

Figure 4. SEM back scattered image showing predominance of spheroidal and framboidal pyrite (grey) diluting galena (white) in the cleaner concentrate sample.

Figure 5. Factor loadings for Pb-containing principal components arising from the ToF-SIMS data for (A) flotation feed, (B) rougher tails, (C) cleaner tails and (D) cleaner concentrate. The '+' and '–' prior to the species stoichiometry refer to the charge of the ion analysed. Isotopes of Cu, Pb and Zn are indicated by a superscript of the neutron number.

Figure 6. Two selected areas from the flotation feed showing on the left hand side particles with surface concentrations of Cu, Zn and Pb with an example highlighted by a solid circle (*e.g.*, PC 3 and PC 4) and on the right hand side a Pb particle with no correlation to either Zn or Cu (PC 5).

Figure 7. Schematic diagram showing galvanic interaction between galena and pyrite.
Fig. 1

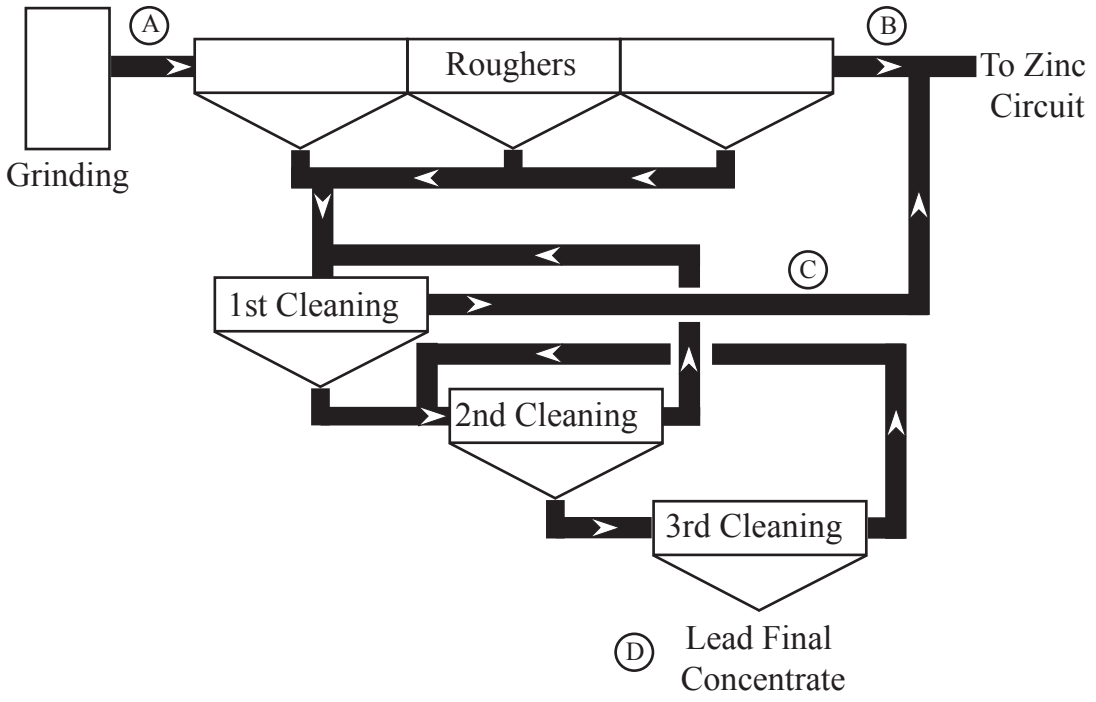
A
B
Roughers
To Zinc
Circuit
Grinding
C
1st Cleaning
2nd Cleaning
3rd Cleaning
D
Lead Final
Concentrate

Fig. 2

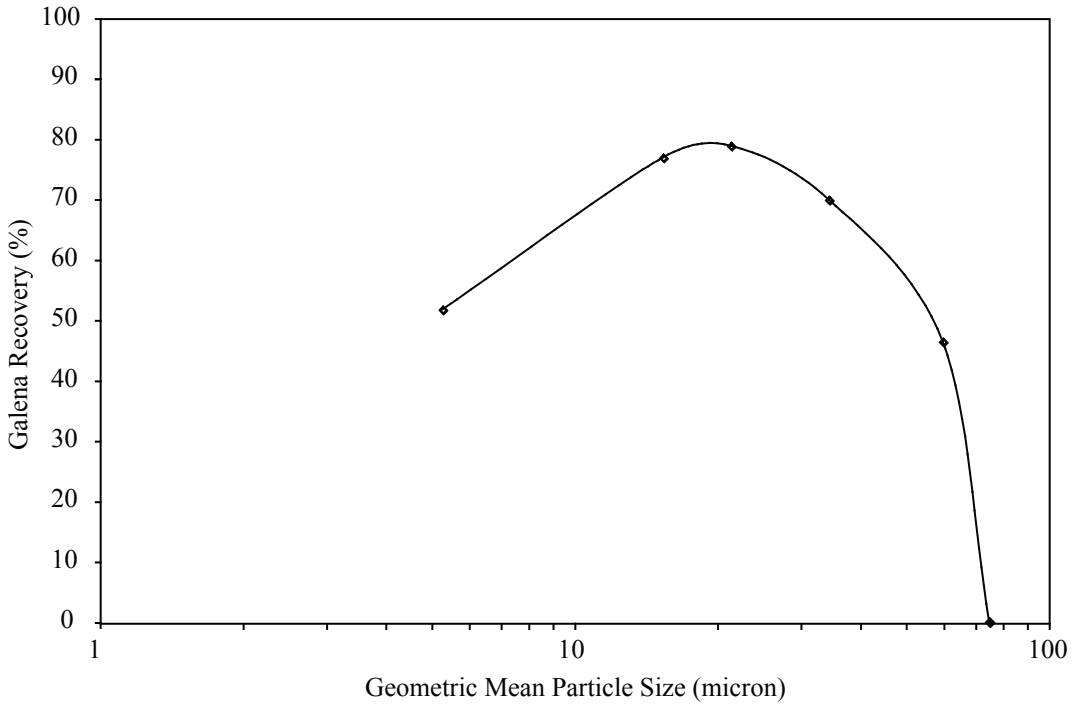
100
90
80
70
60
50
40
30
20
10
0
Galena Recovery (%)
1
10
100
Geometric Mean Particle Size (micron)

Fig. 3

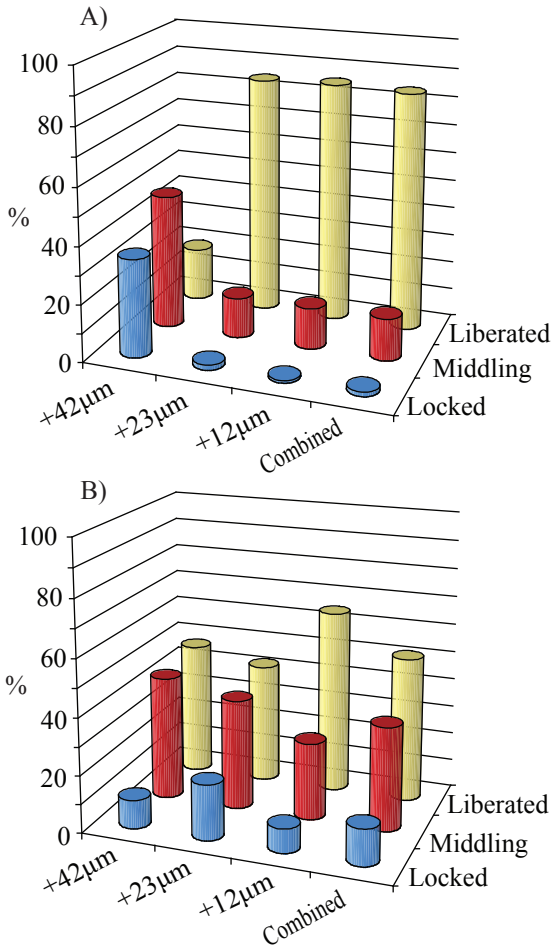
A)
100
80
60
%
40
20
0
+42µm
+23µm
+12µm
Combined
Liberated
Middling
Locked
B)
100
80
60
%
40
20
0
+42µm
+23µm
+12µm
Combined
Liberated
Middling
Locked

Fig. 4

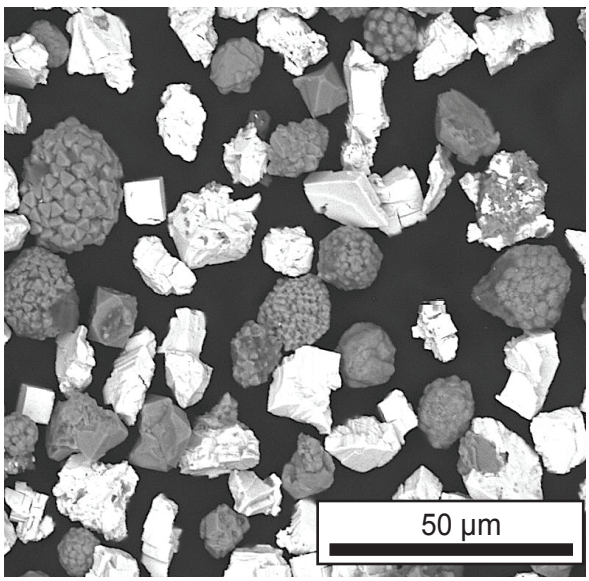
50 µm

Fig. 5

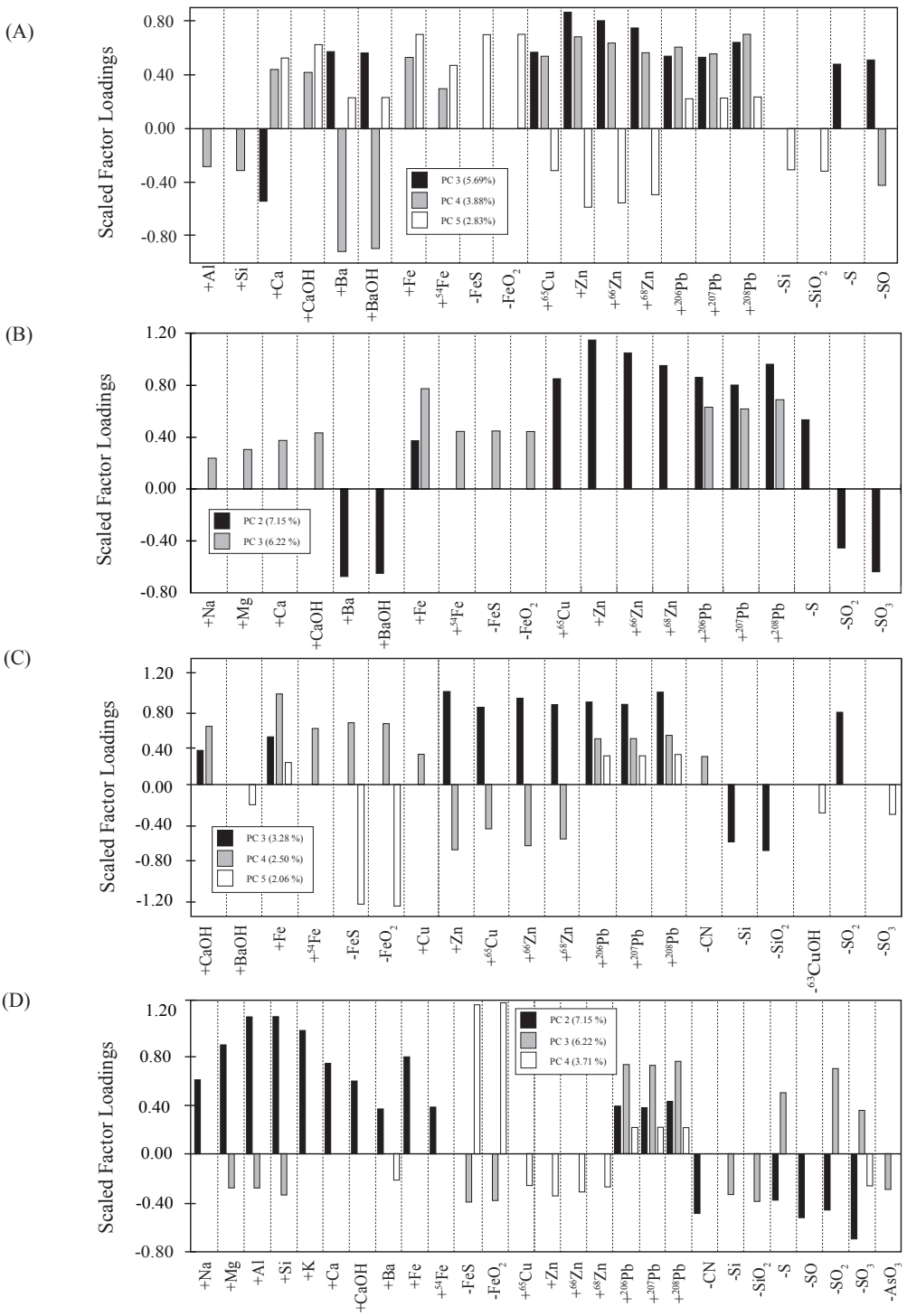
(A)
Scaled Factor Loadings
0.80
0.40
0.00
-0.40
-0.80
PC 3 (5.69%)
PC 4 (3.88%)
PC 5 (2.83%)
+Al
+Si
+Ca
+CaOH
+Ba
+BaOH
+Fe
+54Fe
-FeS
-FeO2
+65Cu
+Zn
+66Zn
+68Zn
+206Pb
+207Pb
+208Pb
-Si
-SiO2
-S
-SO
(B)
Scaled Factor Loadings
1.20
0.80
0.40
0.00
-0.40
-0.80
PC 2 (7.15 %)
PC 3 (6.22 %)
+Na
+Mg
+Ca
+CaOH
+Ba
+BaOH
+Fe
+54Fe
-FeS
-FeO2
+65Cu
+Zn
+66Zn
+68Zn
+206Pb
+207Pb
+208Pb
-S
-SO2
-SO3
(C)
Scaled Factor Loadings
1.20
0.80
0.40
0.00
-0.40
-0.80
-1.20
PC 3 (3.28 %)
PC 4 (2.50 %)
PC 5 (2.06 %)
+CaOH
+BaOH
+Fe
+54Fe
-FeS
-FeO2
+Cu
+Zn
+65Cu
+66Zn
+68Zn
+206Pb
+207Pb
+208Pb
-CN
-Si
-SiO2
-63CuOH
-SO2
-SO3
(D)
Scaled Factor Loadings
1.20
0.80
0.40
0.00
-0.40
-0.80
PC 2 (7.15 %)
PC 3 (6.22 %)
PC 4 (3.71 %)
+Na
+Mg
+Al
+Si
+K
+Ca
+CaOH
+Ba
+Fe
+54Fe
-FeS
-FeO2
+65Cu
+Zn
+66Zn
+68Zn
+206Pb
+207Pb
+208Pb
-CN
-Si
-SiO2
-S
-SO
-SO2
-SO3
-AsO3

Fig. 6

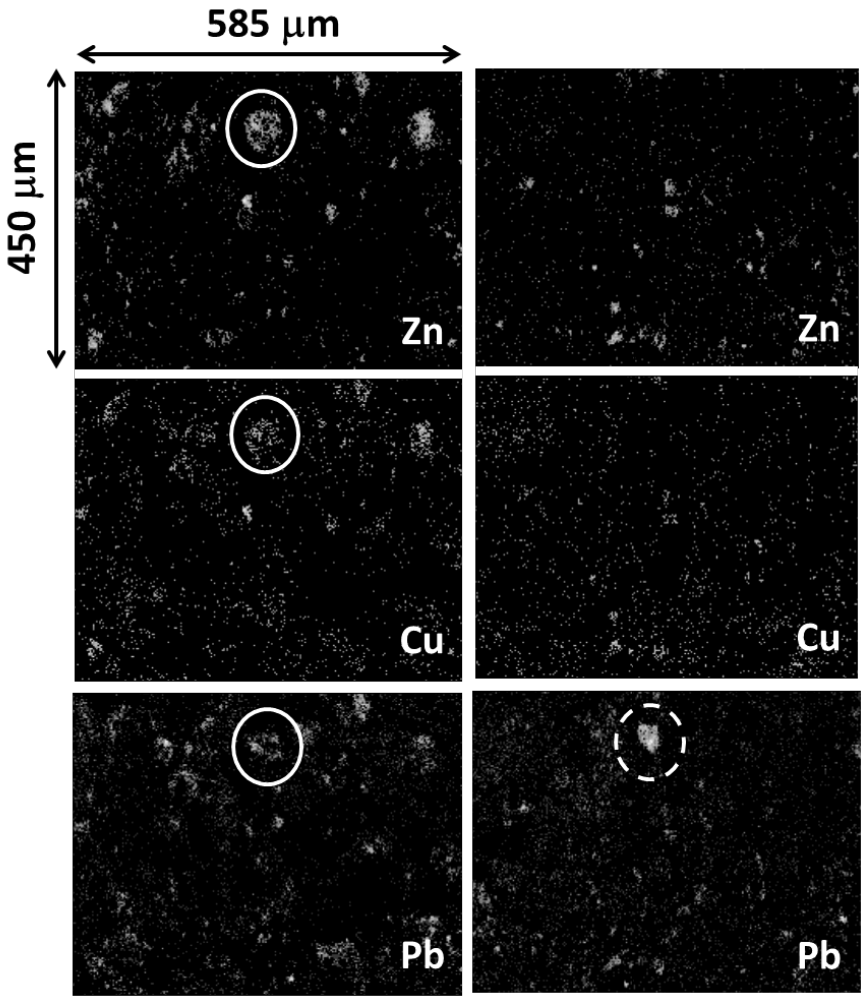
585 µm
450 µm
Zn
Zn
Cu
Cu
Pb
Pb

Fig. 7

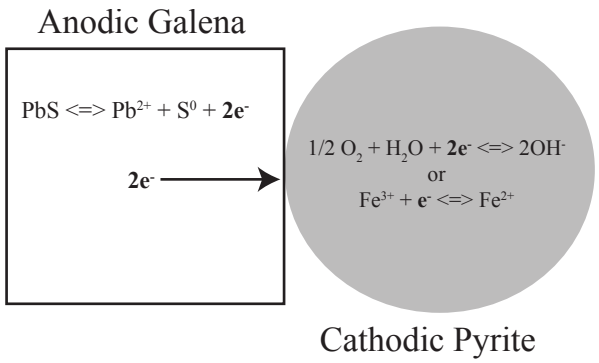
Anodic Galena
PbS <=> Pb2+ + S0 + 2e-
2e-
1/2 O2 + H2O + 2e- <=> 2OH-
or
Fe3+ + e- <=> Fe2+
Cathodic Pyrite

Table 1
Mineral mass (wt.%) for feed, cleaner tails and cleaner concentrate samples.

	Feed	Tails	Concentrate
Pyrite	15.9	67.8	15.9
Pyrite (As)	0.2	0.5	0.1
Galena	3.5	7.0	79.4
Boulangerite*	0.1	0.1	2.1
Sphalerite	12.6	9.0	1.6
Calcite	26.3	5.3	0.3
Dolomite	13.8	2.6	0.0
Ankerite	0.4	0.1	0.0
Quartz	12.1	2.4	0.1
Feldspars	6.3	1.3	0.0
Muscovite	1.7	1.0	0.0
Other Silicates	0.3	0.1	0.0
Barite	5.6	2.1	0.2
Apatite	0.8	0.3	0.0
Others	0.6	0.6	0.2

* Sb-Pb sulfide assumed to be boulangerite composition, $Pb_5Sb_4S_{11}$

Table 2
Liberation and association characteristics of the main sulfide minerals in each of the samples, fraction by fraction (%).

	Feed				Cleaner Tails				Cleaner Concentrate			
Pyrite	+42µm	+23µm	+12µm	Bulk	+42µm	+23µm	+12µm	Bulk	+42µm	+23µm	+12µm	Bulk
Liberated (>90%)	44.0	15.7	12.0	71.7	5.9	33.9	41.2	81.0	0.2	24.2	60.6	85.1
Py+Sph	4.1	0.7	0.5	5.4	0.3	1.8	1.5	3.6	0.0	0.4	0.8	1.3
Py+Gal	0.4	0.1	0.1	0.6	0.2	0.5	0.3	1.0	0.6	2.3	6.1	9.0
Py+Sph+Gal	0.3	0.1	0.0	0.4	0.1	0.1	0.1	0.3	0.1	0.2	0.2	0.4
Py+CO_3	7.3	2.6	1.1	11.0	0.7	3.9	2.5	7.1	0.0	0.5	1.0	1.6
Py+Qtz	0.3	0.2	0.2	0.7	0.1	0.8	0.6	1.5	0.0	0.1	0.3	0.4
Py+Silicates	1.5	1.2	0.8	3.5	0.1	0.3	0.6	1.0	0.0	0.0	0.2	0.2
Complex	4.2	1.4	1.2	6.8	0.4	2.1	2.0	4.5	0.1	0.7	1.2	2.0
Total	62.0	22.0	16.0	100.0	7.8	43.5	48.7	100.0	1.0	28.5	70.4	100.0
Galena												
Liberated (>90%)	31.4	3.7	7.4	42.5	6.9	8.9	17.4	33.2	12.8	19.3	13.3	45.4
Gal+Sb*	35.3	7.1	2.6	45.0	9.8	7.1	5.5	22.4	18.6	19.9	7.6	46.1
Gal+Sph	2.9	1.2	0.3	4.4	8.3	8.2	2.8	19.2	1.6	1.6	0.4	3.6
Gal+Py	2.4	0.5	0.3	3.2	1.7	3.5	3.0	8.1	0.3	0.8	1.6	2.7
Gal+Sph+Py	1.2	0.2	0.1	1.5	1.3	1.5	0.6	3.4	0.1	0.1	0.1	0.2
Pb+CO_3	0.6	0.0	0.3	0.8	1.0	1.1	1.3	3.3	0.3	0.3	0.1	0.7
Pb+Silicates	0.1	0.0	0.1	0.2	0.2	0.1	0.3	0.6	0.0	0.0	0.0	0.1
Complex	1.3	0.6	0.5	2.4	3.2	4.3	2.3	9.7	0.3	0.4	0.5	1.2
Total	75.1	13.4	11.6	100.0	32.5	34.6	33.0	100.0	34.1	42.4	23.5	100.0

* Sb-Pb sulfide assumed to be boulangerite composition, $Pb_5Sb_4S_{11}$